JOURNAL OF CATALYSIS 149, 223–228 (1994)

On the Compact Structure of Small fcc Metal Clusters

Liqiu Yang and Andrew E. DePristo

Ames Laboratory, USDOE; and Department of Chemistry, Iowa State University, Ames, Iowa 50011

Received February 2, 1994; revised June 6, 1994

The general structure of small fcc metal clusters was investigated through the use of site energies, i.e., interaction energy per atom as a function of coordination. We used *only* experimental data on the dimer binding energy, the surface energy, and the bulk cohesive energy to determine these energies for all 15 fcc metals. These showed that real fcc metal systems exhibit a slight bond weakening as the number of bonds increases. It is also demonstrated that experimental data are much closer to the limit of constant bond energy than to that of constant interaction energy per atom. The constant bond energy model leads to compact structures which maximize the number of bonds, and thus we predicted that real small cluster systems would also be compact. Using molecular dynamics/Monte Carlo corrected effective medium theory, which nearly duplicates the experimental site energy curves, we studied the structures of 13-atom clusters of fcc metals via repeated melting and quenching in computer simulations. The lowest-energy structure was found to be a compact icosahedron with very high symmetry in every case. We also performed such simulations in the presence of a SiO_2 support and found that the 13-atom Pt cluster maintained its nearly icosahedral shape. © 1994 Academic Press, Inc.

I. INTRODUCTION

Supported metal catalysts are used widely in the automobile and petroleum industries for a variety of catalytic reactions. One open question about these catalysts is whether they have well-defined shapes and structures.

Earlier observations by transmission electron microscopy (TEM) normal to the metal–support interface displayed the crystalline shape of very large (i.e., diameter >300 Å) metal clusters (1). More recent experiments have provided evidence for well-defined symmetric structures of small (<200 atoms) metal clusters using various molecular and atomic adsorbate probes (2), but such findings have been argued to be caused by the probes (3).

Delocalized electronic bonding in metals requires a description using many-body potentials (4–16). A recent study using the corrected effective medium (CEM) theory (4–11) demonstrated that 13-atom clusters for Ni and Pd were compact icosahedral structures (11). Another work used the effective medium (EM) theory, which included a one-electron term via a tight-binding Hamiltonian having one electronic state per atom (4*s* for Cu), and produced a nearly spherical close-packed 13-atom Cu cluster (12). The more accurate self-consistent local density functional Carr–Parrinello method predicted that, for the 13-atom Al cluster, a single well-defined minimum energy structure exists and is a slightly Jahn–Teller distorted icosahedral structure (13). By contrast, a recent study using the embedded atom method (EAM) (14) found that the 13-atom Pt cluster prefers several completely distorted structures much different from the icosahedral structure (15). Later, another EAM work pointed out that other fcc metals (besides Pt) prefer to have 13-atom icosahedral structures (16).

In order to understand these very different behaviors and especially to determine which theoretical results describe real systems accurately, we have recently investigated the case of 13-atom Pt clusters using two similar many-body potentials generated from the molecular dynamics/Monte Carlo corrected effective medium (MD/MC-CEM) theory (8). One predicted compact icosahedral structure with very high symmetry, while the other predicted open and fluxional structures with low symmetries (17). As compared to the experimental data, the former reproduces the dimer and surface energies reasonably well, while the latter is in error by more than a factor of 2 for these quantities. We concluded that physical reality is most likely to be modeled by the potential which produces the icosahedral structure for the 13-atom Pt cluster.

In this paper, we provide an analysis of cluster structure based upon the much simpler concept of site energy, i.e., interaction energy per atom as a function of coordination (18–22). We use the available experimental information on dimer, surface, and bulk energies to calibrate the coordination dependence of these site energies for all 15 fcc metals: Al, Ca, Ni, Cu, Sr, Rh, Pd, Ag, Ce, Yb, Ir, Pt, Au, Pb, and Th. By comparison to the structures prediced by the MD/MC-CEM theory which provides accurate dimer, surface, and bulk energies, we draw conclusions about which metals are most likely to have fluxional structures if such structures do exist in small catalysts. Finally, we also discuss the effects of the support (SiO_2) and the

0021-9517/94 $6.00

lattice-size mismatch (in bimetallic systems) on the shape of metal catalysts.

II. METHODOLOGY, RESULTS, AND DISCUSSIONS

To analyze the binding characteristics of fcc metals most simply, we use the concept of site energies (17–22). This approach has been detailed previously, especially in Ref. (18), and thus we provide only a brief overview. For a system of N atoms, $\{A_i, i = 1, \ldots, N\}$, the interaction energy is

$$\Delta E(\{A_i\}) = \sum_{i=1}^{N} \varepsilon(A_i; C_i), \qquad [1]$$

where $\varepsilon(A_i; C_i)$ is the site energy *per atom* for atom A_i with C_i nearest neighbors. C_i is referred to as the coordination number of atom A_i. This description is applicable to the close-packed fcc and nearly ideal hcp ($c/a \approx 1.633$) metals in regular arrangements, since Eq. [1] includes the dominant effect of significant variation of atomic stability with number of neighbors. This formula does not assume either pairwise additive interactions or constant bond energies. Equation [1] is not applicable when other effects, such as directional bonding, dominate.

The site energies were determined from experimental data as follows. For $C = 1$, an atom has one nearest neighbor and thus $\varepsilon(A_i; 1) = -D_0/2$, where D_0 is the experimental dimer dissociation energy (23, 24). For $C = 9$, an atom has nine nearest neighbors and thus $\varepsilon(A_i; 9)$ was set equal to the interaction energy of an atom in the top layer of the (111) surface. This energy is just the sum of the bulk interaction energy, $-E_{\text{coh}}$, and the surface energy at 0 K, $\sigma(111)$, multiplied by the area per atom on the (111) surface, $(3^{1/2}/4)a_0^2$, where a_0 is the lattice constant. The contribution from subsurface layers to the surface energy is negligible for the close-packed (111) face (9). Most experimental surface energies were taken from Ref. (25) and extrapolated to 0 K (9), except those for Ca, Sr, Yb, Ir, and Au, which were taken from Ref. (26), and that for Pb, which was taken from Ref. (27). Finally, for $C = 12$, an atom has 12 nearest neighbors and thus $\varepsilon(A_i; 12) = -E_{\text{coh}}$ (28).

In Fig. 1, we show the site energies for Al, Ca, Ni, Cu, Sr, Rh, Pd, Ag, Ce, Yb, Ir, Pt, Au, Pb, and Th. The values at $C = 1$ are unavailable for Sr and Th those at $C = 9$ are unavailable for Ce and Th. The metals with such incomplete data are shown as solid symbols in Fig. 1. The value at $C = 1$ for Ir is the only nonexperimental result in Fig. 1, which was taken as the average of four other empirical estimates by Morse (24). The three data points for each metal fall almost on a straight line, with Al exhibiting the most deviation. This suggests a very simple linear dependence of site energy upon the coordination ($1 \le C_i \le 12$), with a *nonzero* constant term,

$$\varepsilon(A_i; C) = \varepsilon_0(A_i) + \alpha(A_i)C. \qquad [2]$$

The two parameters, $\varepsilon_0(A_i)$ and $\alpha(A_i)$, may depend on the chemical identity of the atom but not on the coordination.

In Fig. 2, we present the scaled site energies, $\varepsilon(A_i; C_i)/|\varepsilon(A_i; 12)|$. The very congested data demonstrate that all of the fcc metals are very similar. (The reader should not be concerned about following each curve since the raw data are in Fig. 1, which can be followed easily.) The two extreme limits shown as dashed lines are as follows: (1) the site energy is directly proportional to the coordination number, $\varepsilon_0(A_i) = 0$, and (2) the site energy is a constant, $\alpha(A_i) = 0$. In the former case, a metal–metal bond has the same energy irrespective of the number of metal–metal bonds; this would produce a 'compact' structure since this maximizes the number of metal–metal bonds, and is labeled as such in Fig. 2. In the latter case, the metal–metal bond weakens inversely proportional to the number of neighbors (i.e., the total bond strength of any atom is constant); this would produce an 'open' and fluxional structure since each atom has the same energy irrespective of the number of neighbors, and is labeled as such in Fig. 2. The experimental data in Fig. 2 lie very close to the 'compact' line and far from the 'open' line, indicating that real fcc metal clusters will have relatively compact structures. *The general variation of data in Fig. 2 indicate that real metal–metal bonds weaken slightly with increasing number of neighbors.*[1]

At this point, we have completed the description using site energies and experimental data. We still want to make a connection to the predictions of atomistic simulations based upon many-body potentials. This is accomplished through the curve labeled "Pt test potential" in Fig. 2, which will provide a close connection between the prediction of model potentials and the site energy curves. Thus, we now describe the many-body potential that was used to investigate the detailed atomic structures of these metal clusters.

We used the non-self-consistent electron density functional CEM theory (4–10) in its simplest framework, the MD/MC-CEM method (8). The interaction energy of a system containing N atoms, relative to the state in which all atoms are infinitely far apart, is given by

$$\Delta E(\{A_i\}) = \sum_{i=1}^{N} \Delta F_{\text{EXLM}}(A_i; n_i) + \tfrac{1}{2}\sum_{i=1}^{N}\sum_{j\neq i} V_c(i,j), \qquad [3]$$

[1] The exceptions occur at $C = 1$ for Ca and Yb. The electronic configurations of Ca ([Ar]$4s^2$) and Yb([Xe]$4f^{14}6s^2$) have completed sub-shells, which yield very weakly bound van der Waals dimers, not chemically bound diatomic molecules.

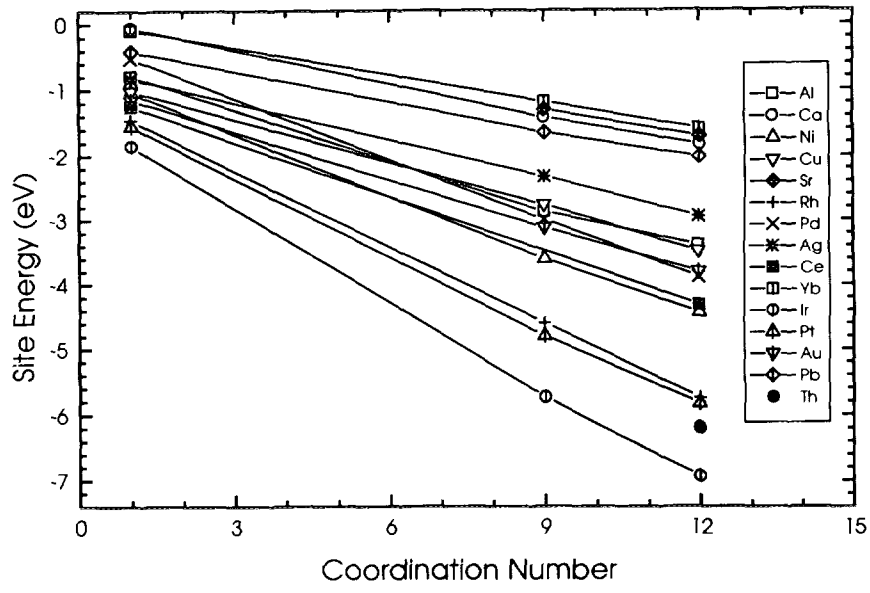

FIG. 1. The site energy (i.e., the interaction energy per atom) in Eq. [1] as a function of the coordination number for 15 fcc metals as determined from experimental data (23–28).

where $\Delta F_{\mathrm{EXLM}}(A_i; n_i)$ is the 'effective' embedding energy of atom A_i into a homogeneous electron gas of electron density, n_i. The jellium electron density surrounding atom A_i is

$$n_i = \tfrac{1}{2} \sum_{j \neq i}^{N} \int \frac{n(A_i; \mathbf{r} - \mathbf{R}_i)}{Z_i} n(A_j; \mathbf{r} - \mathbf{R}_j)\, d\mathbf{r}, \qquad [4]$$

where $n(A_i; \mathbf{r} - \mathbf{R}_i)$ is the atomic electron density for atom A_i with atomic number Z_i and nuclear position $\mathbf{R}_i$. The atomic electron densities were obtained from Hartree–Fock calculations (29, 30).

In Eq. [3], the $V_c(i, j)$ term is the Coulomb interaction energy, which depends only upon the already specified atomic electron density. The only adjustable part in Eq. [3] is $\Delta F_{\mathrm{EXLM}}(A_i; n_i)$, which was constructed by forcing the MD/MC-CEM result to duplicate both the linear muffin tin orbital (LMTO) calculated bulk cohesive energy

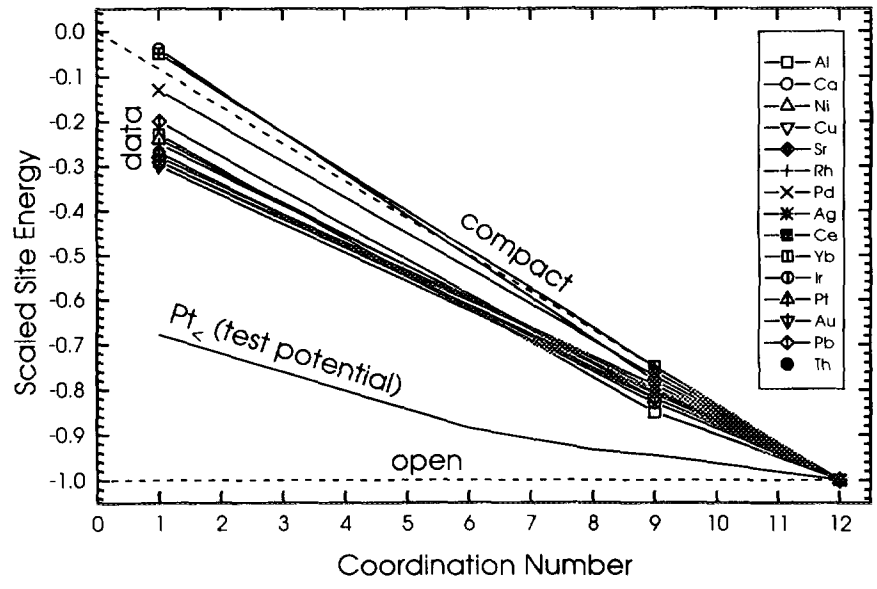

FIG. 2. The scaled site energy, $\varepsilon(A_i, C_i)/|\varepsilon(A_i, 12)|$, determined from the data in Fig. 1 as a function of the coordination number (23–28). The dashed lines, passing through the origin and horizontal, enclose the typical regions for the site energies of real metals.

curve (9) and the dimer binding curve (10). The only two exceptions are Ir and Rh, for which no dimer information was incorporated, due to the lack of data for the former and the questionable experimental result for the latter (24). The surface energies are consistently about 10–15% too low compared to the experimental data (9). As such, the MD/MC-CEM generated potentials provide very good agreement with the experimental data in Fig. 1.

With the above atomistic potentials we performed structural optimization to elucidate the detailed structures of metal clusters and in order to have confidence that the results would describe real metals. We focused on the 13-atom clusters and performed structural optimization of these by simulated annealing using Langevin molecular dynamics. Details of Langevin dynamics can be found in Ref. (31) and we provide only a brief overview here. Each atom evolves according to Newton's equations using the force from the gradient of the interaction potential, but in addition, each atom has an added frictional force proportional to the velocity and a Gaussian random white noise force. The strength of the random force is chosen to exactly balance the dissipative frictional velocity force at a given temperature. The heating cycle is then accomplished by increasing the strength of the random force to slowly increase the average kinetic energy of the atoms in the cluster until the cluster melts. At this temperature, we stopped heating the cluster atoms and just followed their motions for a long time. Periodically, we quenched the structure by removing the random forces and letting the frictional forces dissipate the kinetic energy. The conjugate gradient method, which uses an approximate second derivative matrix, was used to find the minimum energy structure once a low temperature was reached. In all quenches, the structures were optimized until the maximum force on any atom was less than 1×10^{-5} eV/bohr.

The above procedure has a very good probability of finding the global minimum. The initial structure was one center atom surrounded by its 12 nearest neighbors at the fcc lattice sites.

The MD/MC-CEM potential for each fcc metal produced an icosahedral 13-atom cluster as the lowest-energy structure. This makes eminent sense since this cluster is quite compact. The icosahedral structure has one atom at the center and one atom at each of the 12 equivalent vertices of an icosahedron which has 20 faces, each being an equilateral triangle. The side-length of each such triangle is approximately 5.15% greater than the radius of the sphere containing all the vertices. In Table 1, the energies and radii of the icosahedral structures are listed for the nine fcc metals treated by the MD/MC-CEM potentials: Al, Ni, Cu, Rh, Pd, Ag, Ir, Pt, and Au. In all cases, the binding energy per atom is substantially below the bulk cohesive energy.

TABLE 1

Interaction Energy and Radius for the Most Stable Icosahedral Structure of the 13-Atom Cluster

Metal	Energy (eV)	Radius (Å)
Al	−31.23	2.54
Ni	−35.50	2.36
Cu	−28.89	2.50
Rh	−46.46	2.53
Pd	−30.05	2.59
Ag	−25.49	2.73
Ir	−57.56	2.52
Pt	−52.14	2.62
Au	−31.67	2.70

Note. Calculated using the MD/MC-CEM potential with the ΔF_{EXLM} embedding function developed in Ref. (6g) that incorporates dimer and bulk data.

The only peculiar point in Table 1 is that Al (−31.23 eV) is bound slightly more strongly than Cu (−28.89 eV) in the cluster even though Al is bound weaker than Cu in the bulk. This is an artifact of the flatness of $\Delta F_{\text{EXLM}}(\text{Al}; n)$ in the jellium density region between the dimer and the bulk, and is discussed in more detail elsewhere (22).

As a further demonstration of the predictive ability of the data in Figs. 1 and 2, we recently constructed a test potential for Pt (denoted as $\text{Pt}_<$ in Ref. (17)) that produced the scaled site energy curve labeled "Pt test potential" in Fig. 2. This potential yielded a Pt dimer interaction energy of −7.91 eV as compared to −3.73 eV from the experiment (23, 24). This potential also yielded a Pt(111) surface energy of 0.81 J/m^2 as compared to 2.49 J/m^2 from experiment (25–27) and to 2.19 J/m^2 for the MD/MC-CEM potential from Eq. [3] used in the present work. Thus, the Pt test potential severely underestimates the surface energy as well; or equivalently, it severely overestimates the binding strength of 9-coordinated atoms on the (111) surface. These are very similar to the problems of the Pt potential used in Ref. (15); the dimer binding energy is around −7.8 eV (16) and the (111) surface energy is 1.44 J/m^2 (14).

The Pt test potential produced nonicosahedral and fluxional 13-atom structures (17). These are merely consequences of the unrealistically strong bonds at lower coordinations associated with the test potential for Pt, as is evident in Fig. 2. Apparently, the fluxional clusters produced by the Pt potential used in Ref. (15) are also consequences of such unrealistically strong bonds. It is necessary to calibrate any potential against available experimental data such as surface energies and dimer binding energies, and the plot in Fig. 2 provides a very concise way to ascertain the general structure features from such a comparison.

Based upon all the data and the trends we found in our simulations, we believe that the most plausible structure for a 13-atom cluster of real fcc metals (including for Pt) is icosahedral, at least in the gas phase. Of course, slight Jahn–Teller distortion from the icosahedral structure is possible (12, 13). Such slightly distorted structures are still very compact and have nearly identical atomic coordinations as a perfect icosahedron.

With the above atomistic validation of the trends in Fig. 2, we can make further predictions. Since the 13-atom cluster is a special size that prefers the icosahedral structure most strongly, clusters of other sizes may have nonicosahedral structures. From Fig. 2, we predict that these will still be rather compact. In addition, we can distinguish among the metals. For example, based upon the experimental information in Fig. 2, that Pt has the strongest and Ca has the weakest relative binding strength at lower coordinations, we expect the degree of compactness to be a maximum for Ca and a minimum for Pt among the fcc metals shown. This does not mean that the Pt clusters will be open and/or fluxional, just that they may not be as compact as the Ca clusters.

In applications, small metal clusters are present on supports such as SiO_2. We can utilize the MD/MC-CEM theory to investigate the effects of the support on these structures. This is intrinsically less accurate than treatment of the isolated metals because the MD/MC-CEM theory utilizes spherical electron densities taken from isolated atoms. The strong directional bonding due to sp^3 hybridization in Si and the electron transfer from Si to O are not included in any way. Thus, we varied a single empirical parameter, β, for the interaction strength between the metal and the SiO_2 support, which is restricted to be *rigid* in the α-quartz structure. This mimics the effect of the support but is clearly not as quantitatively accurate or theoretically justified as the previous applications of MD/MC-CEM to pure metal clusters.

To be specific, $1/\beta$ scales the bulk fitted Si embedding function at a jellium electron density corresponding to 30% contraction of the Si lattice constant. Decreasing β decreases the attraction of a metal cluster with the substrate. We estimated β in the following way. TEM observations (1) of Au particles on alumina heated in air at 900·C for 75 h showed stable, nearly crystalline Au clusters 300–600 Å in diameter supported by the alumina. Because Au presents special problems due to relativistic effects, we did not use this information directly. Instead, we made the reasonable assumption that a similarly inert Ag metal particle around 15 Å in diameter (i.e., ≈200 atoms) would also have definite but minimal contact with the support. By testing $\beta = 1, 0.5, 0.2, 0.1$, and 0.05, we found that $\beta = 0.2$ meets the above expectation very well. For this value, we tested all ten 201-atom 50%–50% bimetallic clusters as selected from the metals Rh, Ni, Pd, Cu, and Ag. At 600 K, these clusters were stably attached to the rigid SiO_2 support in 1-ns simulations without wetting the surface. In one longer simulation for 10 ns at 1000 K, the Rh–Ni cluster was still stable on the support. No further refinement for the value of beta was attempted since these simulations are computer-time-consuming.

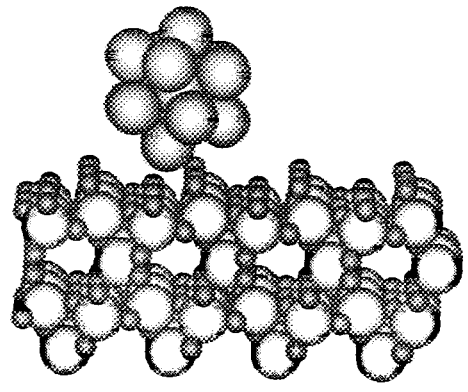

Side View

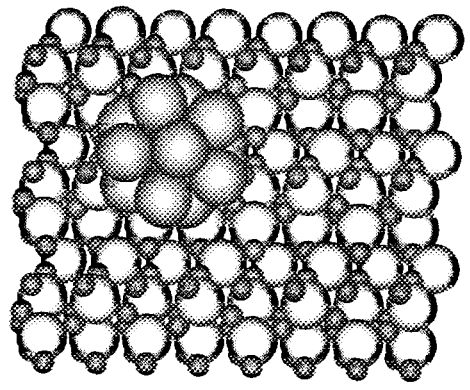

Top View

FIG. 3. The side view and the top view of a 13-atom Pt cluster supported on SiO_2. The large, medium, and small spheres represent Pt, Si, and O atoms, respectively.

Shown in Fig. 3 is the minimum-energy 13-atom Pt cluster on a rigid SiO_2 support using $\beta = 0.2$. The interaction energy between the cluster and the support is −0.69 eV, a stable adsorption. Although this cluster is nearly icosahedral, there are no exactly equivalent atoms in the cluster due to lack of symmetry in the system. The longest bond length (2.77 Å) is 6.1% longer than the shortest (2.61 Å), as compared to 5.15% for a perfect icosahedron. Such slight deformation from the icosahedral structure only increases the energy of the isolated cluster by 8 meV as compared to −52.14 eV in Table 1 for Pt.

III. CONCLUSIONS

The experimental site energies for fcc metals displayed a monotonic and nearly linear decrease with increasing coordination. This behavior causes real metal clusters to form compact structures which maximize the total coordination of the atoms. The MD/MC-CEM potential, which generates site energies in very close agreement with experiment, was used for atomistic simulations of the structure of small metal clusters. For the case of the 13-atom cluster of fcc metal atoms, the MD/MC-CEM potential generated a very plausible ground state structure: an icosahedron. Higher level theories may introduce small perturbations to the perfect structure due to the Jahn–Teller distortion, but will not change the general trend toward compact structures. On the other hand, an interaction potential that is not well-calibrated may produce many other types of structures with little relevance to real metallic systems.

Clusters of other sizes may have nonicosahedral structures, of course, but we predicted that these would still be rather compact. In addition, we showed that the degree of compactness would be a maximum for Ca and a minimum for Pt among the fcc metals. This does not mean that the Pt clusters will be open and/or fluxional, just that they may not be as compact as the Ca clusters. Indeed, atomistic simulations on the 13-atom Pt cluster yielded a very stable icosahedral ground state compact structure.

Based upon atomistic simulations, we found no evidence for strong distortion of the icosahedral structure for the 13-atom Pt cluster due to the presence of a SiO_2 support. While the general trend of compact cluster structure pertains only to pure metals, we also expect this to hold for multimetallic clusters if the metals are mismatched in lattice size by a small amount, say less than 10%. For such small mismatches, atomistic simulations indicate that regular cubo-octahedral structures are retained for 201-atom clusters (21, 22). For larger size mismatches, our previous simulations have shown severe deformation of the initial cubooctahedral shape for Ni–Ag and Cu–Ag clusters, which have 15 and 12.5% lattice-size mismatches, respectively (21, 22). No matter how symmetric and compact the monoatomic metal clusters are, the shape of a largely mismatched dimetallic cluster is completely distorted and may not be compact for the surface species.

ACKNOWLEDGMENTS

We thank Professor T. S. King for discussions and Dr. F. Liu for providing a subroutine to generate the α-quartz structure. This work was supported by the Biological and Chemical Technologies Research Program (Advanced Industrial Concepts Division) and the Division of Chemical Sciences, Office of Basic Energy Sciences, of the U.S. Department of Energy through the Ames Laboratory, which is operated for the U.S. DOE by Iowa State University under Contract No. W-7405-Eng-82.

REFERENCES

1. Pilliar M., and Nutting, J., *Philos. Mag.* **16,** 181 (1967).
2. Klots, D., Winter, B. J., Parks, E. K., and Riley, S. J. *J. Chem. Phys.* **95,** 8919 (1991), and references therein.
3. Masel, I., private communication at the 13th North American Meeting of the Catalysis Society, Pittsburgh, PA, May 1993.
4. Kress, J. D., and DePristo, A. E., *J. Chem. Phys.* **87,** 4700 (1987).
5. Kress, J. D., and DePristo, A. E., *J. Chem. Phys.* **88,** 2596 (1988).
6. Kress, J. D., Stave, M. S., and DePristo, A. E., *J. Phys. Chem.* **93,** 1556 (1989).
7. Raeker, T. J., and DePristo, A. E., *Int. Rev. Phys. Chem.* **10,** 1 (1991).
8. Stave, M. S., Sanders, D. E., Raeker, T. J., and DePristo, A. E., *J. Chem. Phys.* **93,** 4413 (1990).
9. Sinnott, S. B., Stave, M. S., Raeker, T. J., and DePristo, A. E., *Phys. Rev. B* **44,** 8927 (1991).
10. Kelchner, C. L., Halstead, D. M., Perkins, L. S., Wallace, N. M., and DePristo, A. E., *Surf. Sci.* **310,** 425 (1994).
11. Stave, M. S., and DePristo, A. E., *J. Chem. Phys.* **97,** 3386 (1992).
12. Christensen, O. B., Jacobsen, K. W., Norskov, J. K., and Manninen, M., *Phys. Rev. Lett.* **66,** 2219 (1991).
13. Yi, J.-Y., Oh, D. J., and Bernholc, J., *Phys. Rev. Lett.* **67,** 1594 (1991).
14. Foiles, S. M., Baskes, M. I., and Daw, M. S., *Phys. Rev. B* **33,** 7983 (1986).
15. Sachdev, A., Masel, R. I., and Adams, J. B., *J. Catal.* **136,** 320 (1992).
16. Vlachos, D. G., Schmidt, L. D., and Aris, R., *Z. Phys. D* **26,** S156 (1993).
17. Yang, L., and DePristo, A. E., *J. Chem. Phys.* **110,** 725 (1994).
18. Strohl, J. K., and King, T. S., *J. Catal.* **116,** 540 (1989).
19. Yang, L., Raeker, T. J., Schoeb, A. M., Wu, X., King, T. S., and DePristo, A. E., *Am. Chem. Soc. Div. Fuel Chem.* **37,** 324 (1992).
20. Schoeb, A. M., Raeker, T. J., Yang, L., Wu, X., King, T., and DePristo, A. E., *Surf. Sci. Lett.* **278,** L125 (1992).
21. Yang, L., Raeker, T. J., and DePristo, A. E., *Surf. Sci.* **290,** 195 (1993).
22. Yang, L., and DePristo, A. E., *J. Catal.*, in press.
23. Huber, K. P., and Herzberg, G., *in* "Molecular Spectra and Molecular Structure" Vol. 4, Constants of Diatomic Molecules, Van Nostrand, Princeton, NJ, 1979.
24. Morse, M., *Chem. Rev.* **86,** 1049 (1986).
25. Mezey, L. Z., and Giber, J., *Jpn. J. Appl. Phys.* **21,** 1569 (1982).
26. de Boer, F. R., Boom, R., Mattens, W. C. M., Miedema, A. R., and Niessen, A. K., "Cohesion in Metals." North-Holland, Amsterdam, 1988.
27. Kumikov, V. K., and Khokonov, K. B., *J. Appl. Phys.* **54,** 1346 (1983).
28. Kittel, C., "Introduction to Solid State Physics." 6th ed., Wiley, New York, 1986.
29. Clementi, E., *IBM J. Res. Dev. Suppl.* **9** (1965).
30. Bagus, P. S., Gilbert, T. L., and Roothan, C. J., *J. Chem. Phys.* **56,** 5195 (1972).
31. DePristo, A. E., and Metiu, H., *J. Chem. Phys.* **90,** 1229 (1989).